

Influence of crystallite size on sputtering coefficients of tungsten bombarded by hydrogen isotopes and argon

© A.V. Smaev, V.S. Mikhailov, P.Yu. Babenko, A.N. Zinoviev

Ioffe Institute, St. Petersburg, Russia
E-mail: zinoviev@inprof.ioffe.ru

Received June 4, 2024

Revised August 13, 2024

Accepted September 12, 2024

Using the code we have developed, we obtained for the first time coefficients Y of the tungsten target sputtering by hydrogen isotopes and argon with the bombarding particle energies ranging from 0.01 to 100 keV in dependence on the crystallite size and type of the surface potential barrier. Numerical simulation has predicted that, when energies exceed 100 eV, a significant increase in the sputtering coefficient is observed with increasing crystallite size. The most remarkable growth takes place while the crystallite size increases from one to two lattice constants. A strong influence of the choice of the surface barrier type on the sputtering coefficient calculations has been demonstrated. The results obtained are necessary for analyzing the entry of tungsten impurities into the tokamak plasma hot region.

Keywords: sputtering coefficients, interatomic interaction potential, hydrogen isotopes, argon, tungsten, crystallite size.

DOI: 10.61011/TPL.2025.01.60149.20009

At present, controlled thermonuclear fusion is regarded as a promising alternative source of power. To succeed in its implementation, it is necessary to overcome a number of technological and technical difficulties. The most important problem on this way is associated with the issues of durability of structural components facing the burning plasma. Surfaces of the first wall and divertor are liable to irradiation by flows of fast atoms, neutrons and plasma. Interaction of high-energy plasma flows with the first wall and other structural components of the tokamak reactor can promote sputtering of these components, modification of their structure, and even their destruction [1,2], as well as entering of impurities into the reactor working volume [3–6]. Especially high load will be applied to the divertor surface [7,8]. Sputtered first-wall particles may reach the last closed magnetic surface (separatrix) and penetrate into the plasma-column central part thus giving rise to high radiative-energy losses.

As a material for the ITER tokamak divertor, it is planned to use one of the most refractory metals, i.e. tungsten characterized by a low sputtering coefficient and high sputtering energy threshold. However, tungsten has such a drawback as large atomic number $Z = 74$ due to which emission of tungsten ions causes large energy losses. When the tungsten concentration is as low as $\sim 0.1\%$ [9], achievement of a high energy efficiency of thermonuclear fusion is impossible.

Entry of impurities into the reactor plasma can significantly change the tokamak operating mode; thus, it is necessary to exactly know and control the flows of incoming impurities. This requires data on sputtering coefficients of tungsten bombarded by hydrogen isotopes, as well as by argon that may be added to plasma in order to

decrease its near-wall temperature. By this moment, those coefficients have been measured only in a limited energy range. Moreover, measurements obtained by different research teams contradict each other. Data for tritium are unavailable.

As the first-wall and divertor material, polycrystalline tungsten is planned to be used. The surface topology can considerably affect the first-wall sputtering. It was shown in [10] that the coefficient of sputtering by He and Ar ions varies strongly depending on orientation of the W crystal-lattice face. Paper [11] showed that sputtering coefficients of tungsten bombarded by Ga ions differ from each other by eight times for different surface orientations. The average sputtering coefficient for the faces of different orientations differs from that for amorphous material. Much attention is paid to sputtering of tungsten fuzz, that is, columnar structures emerging on the surface under an intense ion-beam bombardment [12,13]. An additional global reduction in the sputtering yield was revealed, which we attributed to the influence of the effect of redeposition between nanocolumns. These results confirm the possibility of using nanocolumnar tungsten as a coating for the tokamak first wall.

The sputtering coefficient dependence on crystallite size has not been studied so far, although the influence of surface topology on the sputtering coefficient has been already mentioned (see, e.g. [10–13]). Among the objectives of this work there was obtaining data on sputtering coefficients Y of tungsten bombarded by argon and hydrogen isotopes (hydrogen, deuterium, tritium) in a wide range of initial energies (0.01–100 keV) for different crystallite sizes.

To describe particles sputtering under bombardment of a solid, we used our own program code based on

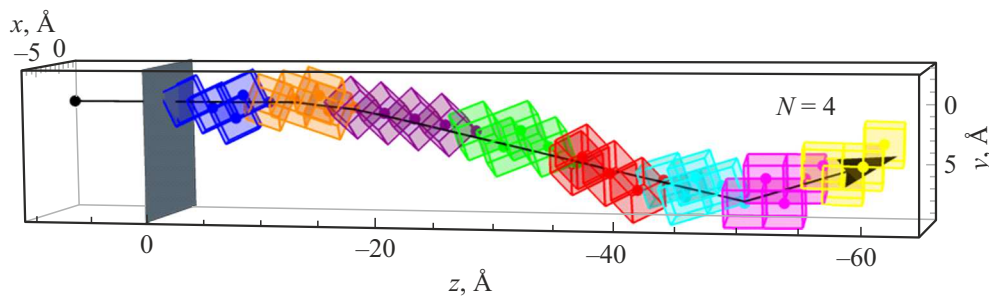


Figure 1. Visualization of the program code operating mode with $N = 4$ (the crystallite grain size equals four unit cells). For clarity, thermal vibrations are not considered, and cube clusters are not left-truncated; however, in the process of simulation, all the atoms to the left of the gray plane (with coordinates $z < 0$) were truncated. Colored dots indicate the cluster atoms where binary elastic collisions occur. Clusters belonging to one and the same grain are colored identically. The black line represents the trajectory of the projectile Ar atom 10 keV in energy; the arrow indicates the motion direction; Ar begins moving from the black dot $(0, 0, 3a)$, where a is the lattice constant. The colored figure is given in the electronic version of the article.

the Monte–Carlo method and binary–collision approximation [14].

The projectile's trajectory was calculated by using potentials obtained in the framework of the Density Functional Theory [15]. The calculations were corrected by the potential-well parameters. Stopping of particles in the target was taken into account. Nuclear stopping power, i.e. energy losses associated with scattering from target atoms, were precisely calculated for the used interaction potential based on the energy and momentum conservation laws. According to the recommendations given in [16], stopping losses on the target electrons were accounted for in the form of a product of the projectile stopping power by the inter-collision distance. Thermal vibrations of target atoms were taken into account; as the vibration amplitude, the value corresponding to room-temperature was taken.

The projectile collision with target atoms gives rise to recoil particles which are able to be emitted beyond the surface boundary provided they overcome the potential barrier at the solid–vacuum interface. In addition, cascade particles generated in the collisions between recoil particles and target atoms were taken into account.

The calculation results strongly depend on the potential barrier model. This model depends on the surface topography. In the case of a severely rough surface consisting of atomic-size peaks, the surface potential may be assumed to be isotropic (spherical). In this case, the sputtered particle energy E_{out} is to be higher than sublimation energy U_s . For a smooth surface, the planar potential model is used. In this case, the sputtered particle should meet condition $E_{out} \cos^2 \theta > U_s$, where θ is the angle of the sputtered particle emission measured from the surface normal.

Under the tokamak's real operating conditions, the surface roughness may vary significantly; therefore, we calculated sputtering coefficients for both the above-considered limiting cases.

Our previous study [17] has shown that the choice of the surface potential model strongly affects the results of calculating the sputtering coefficients.

The target was described by the model within which an atomic cluster one lattice constant in size was used to take into account the correlation in the nearest-neighbor arrangement. Position of the first atom and cluster's spatial orientation were chosen randomly. After the collision, a next cluster was constructed whose center was set to the atom on which the next scattering occurred. At $N = 1$, spatial orientation of this cluster was chosen randomly. At $N \geq 2$, the cluster's spatial orientation was maintained until the particle interacted with the given cluster's number N . After that, the cluster's orientation was chosen randomly again, and again was maintained until number N was reached. Thus, there was created a model of a polycrystalline target with the grain size of N (expressed in the number of unit cells). Crystallite size N was varied from 1 to 100.

Fig. 1 visualizes the mode with $N = 4$ for a randomly selected trajectory.

Fig. 2 demonstrates calculations of sputtering coefficient Y versus collision energy for the case of normal argon-beam incidence on the target surface. Dashed colored lines represent the case of the spherical barrier, solid colored lines are for the planar barrier. Dots are experimental data obtained by different researchers and given in the monograph [18]. The gray dashed-and-dotted line represents the Eckstein team's calculations [18,19]. Figures at the curves indicate the values of crystallite size N . In Fig. 2, *b*, the ordinate-axis scale was made linear in order to make clearer the strong crystallite-size effect on the sputtering coefficient.

As N increases, sputtering coefficients for the Ar–W system increase till $N = 8$ for both potential barrier versions. The figure shows that the planar barrier provides lower coefficients Y . Further increase in the crystallite size ($N > 8$) results in saturation of the Y dependence. The agreement between the experimental data and simulation results is better in the case of the planar barrier. The main factor justifying the planar potential barrier model is the presence of a maximum in the energy distribution of sputtered particles. In the case of the spherical surface

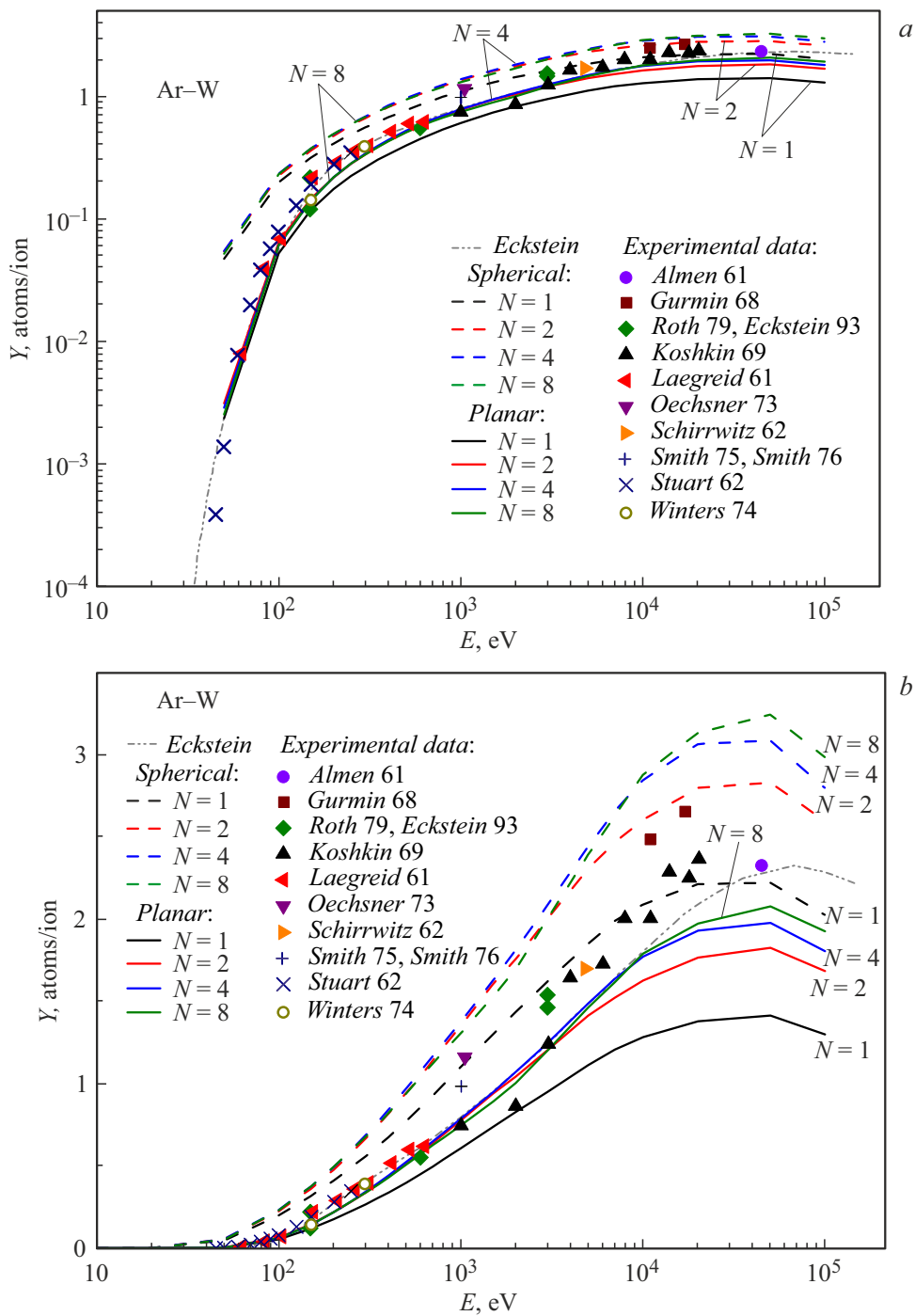


Figure 2. Tungsten sputtering coefficient versus collision energy in the case of normal argon-beam incidence on the target. Dashed colored lines represent our calculations for the spherical barrier, solid colored lines are our calculations for the planar barrier, dots are experimental data, gray dashed-and-dotted line represents the calculations obtained by the Eckstein team. The calculations are presented in double logarithmic coordinates (a) and ordinate-axis linear scale (b). The colored figure is given in the electronic version of the article.

potential, this maximum would appear at the zero energy of sputtered particles, which does not agree with experimental data. In the case of measuring sputtering coefficients for tungsten, it is possible to prepare a sufficiently smooth surface. Intense ion bombardment can make the surface considerably rough.

Fig. 3 demonstrates calculations of sputtering coefficient Y versus collision energy for the case of normal hydrogen-isotope incidence on the target surface. When number N increases, sputtering coefficients for the H–W, D–W, and T–W systems also increase for both potential barrier versions but only up to $N \approx 2$. The planar barrier again

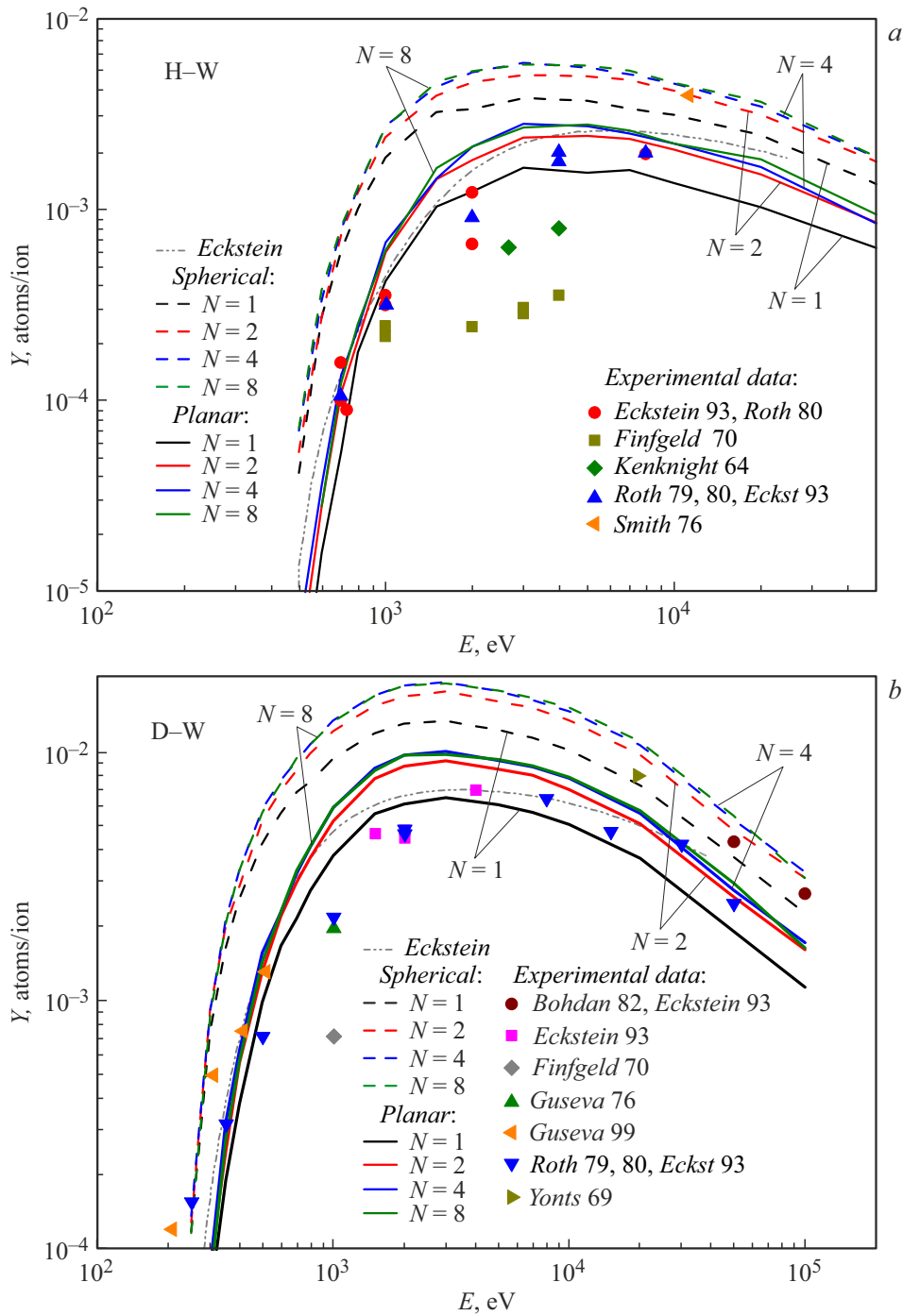


Figure 3. Tungsten sputtering coefficient versus collision energy in the case of normal hydrogen-beam incidence on the target: *a* — H, *b* — D, *c* — T. Dashed colored lines represent our calculations for the spherical barrier, solid colored lines are our calculations for the planar barrier, dots are experimental data, gray dashed-and-dotted line represents the calculations obtained by the Eckstein team. The colored figure is given in the electronic version of the article.

gives lower coefficients Y . When the crystallite size continues increasing ($N > 8$), the Y dependence tends to saturation. Similarly to the case of the Ar–W system, experimental data for the planar barrier are in better agreement with the simulation results.

Thus, it has been established that the sputtering coefficient significantly depends on the target crystallite size; the

most significant variation is observed while the crystallite size increases from $N = 1$ to $N = 2$, after which the growth becomes slower. To our mind, the obtained dependences of sputtering coefficients on the target crystallite size may be associated with manifestations of channeling in the process of recoil particles emission from the target. The results of computer simulation confirm that the depth of the

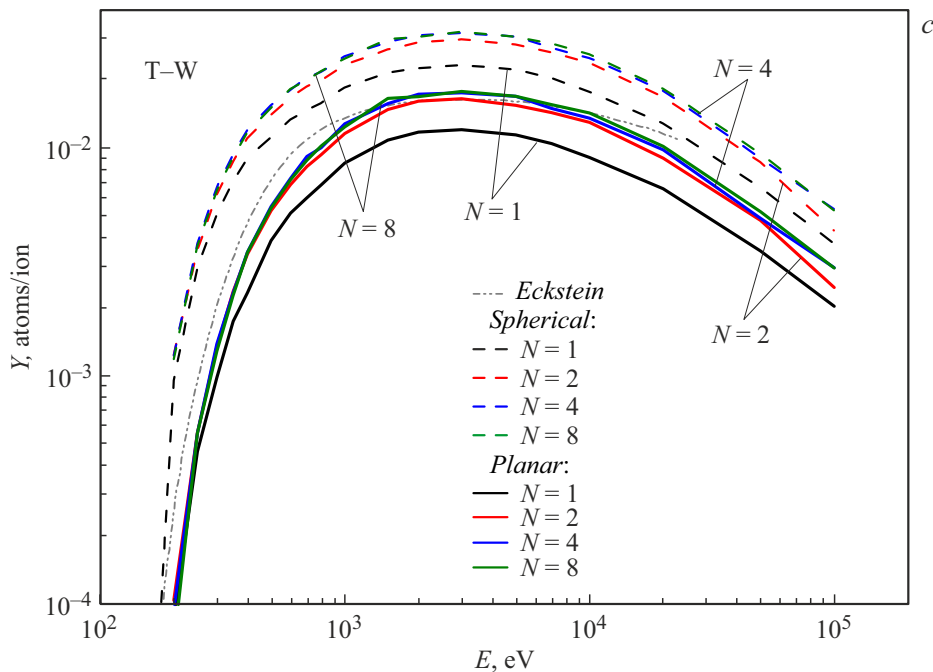


Fig. 3 (continued).

layer wherefrom sputtered atoms are emitted increases with increasing crystallite size.

Conflict of interests

The authors declare that they have no conflict of interests.

References

- [1] J. Linke, J. Du, T. Loewenhoff, G. Pintsuk, B. Spilker, I. Steudel, M. Wirtz, *Matter Rad. Extrem.*, **4**(5), 056201 (2019). DOI: 10.1063/1.5090100
- [2] O. El-Atwani, S. Gonderman, M. Efe, G. De Temmerman, T. Morgan, K. Bystrov, D. Klenosky, T. Qiu, J.P. Allain, *Nucl. Fusion*, **54** (8), 083013 (2014). DOI: 10.1088/0029-5515/54/8/083013
- [3] S. Yamoto, X. Bonnin, Y. Homma, H. Inoue, K. Hoshino, A. Hatayama, R.A. Pitts, *Nucl. Fusion*, **57** (11), 116051 (2017). DOI: 10.1088/1741-4326/aa7fa6
- [4] R.D. Smirnov, S.I. Krashennnikov, A.Yu. Pigarov, T.D. Rognyen, *Phys. Plasmas*, **22** (1), 012506 (2015). DOI: 10.1063/1.4905704
- [5] F. Ding, G.-N. Luo, X. Chen, H. Xie, R. Ding, C. Sang, H. Mao, Z. Hu, J. Wu, Z. Sun, L. Wang, Y. Sun, J. Hu and the EAST Team, *Tungsten*, **1** (2), 122 (2019). DOI: 10.1007/s42864-021-00115-4
- [6] R.A. Pitts, X. Bonnin, F. Escourbiac, H. Frerichs, J.P. Gunn, T. Hirai, A.S. Kukushkin, E. Kaveeva, M.A. Miller, D. Moulton, V. Rozhansky, I. Senichenkov, E. Sytova, O. Schmitz, P.C. Stangeby, G. De Temmerman, I. Veselova, S. Wiesen, *Nucl. Mater. Energy*, **20**, 100696 (2019). DOI: 10.1016/j.nme.2019.100696
- [7] B. Gao, R. Ding, H. Xie, L. Zeng, L. Zhang, B. Wang, C. Li, D. Zhu, R. Yan, J. Chen, *Fusion Eng. Des.*, **156**, 111616 (2020). DOI: 10.1016/j.fusengdes.2020.111616
- [8] J. Guterl, I. Bykov, R. Ding, P. Snyder, *Nucl. Mater. Energy*, **27**, 100948 (2021). DOI: 10.1016/j.nme.2021.100948
- [9] R.V. Jensen, D.E. Post, W.H. Grasberger, C.B. Tarter, W.A. Lokke, *Nucl. Fusion*, **17** (6), 1187 (1977). DOI: 10.1088/0029-5515/17/6/007
- [10] J. Jussila, F. Granberg, K. Nordlund, *Nucl. Mater. Energy*, **17**, 113 (2018). DOI: 10.1016/j.nme.2018.08.002
- [11] K. Schlueter, K. Nordlund, G. Hobler, M. Balden, F. Granberg, O. Flinck, T.F. da Silva, R. Neu, *Phys. Rev. Lett.*, **125** (22), 225502 (2020). DOI: 10.1103/PhysRevLett.125.225502
- [12] A. Lopez-Cazalilla, J. Jussila, K. Nordlund, F. Granberg, *Comput. Mater. Sci.*, **216**, 111876 (2023). DOI: 10.1016/j.commatsci.2022.111876
- [13] A. Lopez-Cazalilla, F. Granberg, K. Nordlund, C. Cepak, M. Fellingner, F. Aumayr, P.S. Szabo, A. Mutzke, R. Gonzalez-Arrabal, *Phys. Rev. Mater.*, **6** (7), 075402 (2022). DOI: 10.1103/PhysRevMaterials.6.075402
- [14] V.S. Mikhailov, P.Yu. Babenko, A.P. Shergin, A.N. Zinoviev, *JETP*, **137** (3), 413 (2023). DOI: 10.1134/S106377612309011X
- [15] A.N. Zinoviev, K. Nordlund, *Nucl. Instrum. Meth. Phys. Res. B*, **406**, 511 (2017). DOI: 10.1016/j.nimb.2017.03.047
- [16] A.N. Zinoviev, P.Yu. Babenko, *JETP Lett.*, **115** (9), 560 (2022). DOI: 10.1134/S0021364022100526
- [17] V.S. Mikhailov, P.Yu. Babenko, A.P. Shergin, A.N. Zinoviev, *Plasma Phys. Rep.*, **50** (1), 23 (2024). DOI: 10.1134/S1063780X23601682
- [18] R. Behrisch, W. Eckstein, *Sputtering by particle bombardment* (Springer, Berlin, 2007). DOI: 10.1007/978-3-540-44502-9
- [19] R.E.H. Clark, *Atomic and plasma-material interaction data for fusion* (IAEA, Vienna, 2001), vol. 7, part B.

Translated by EgoTranslating